



## CH<sub>4</sub> and N<sub>2</sub>O fluctuations during the penultimate deglaciation

Loïc Schmidely, Christoph Nehrbass-Ahles, Jochen Schmitt, Juhyeong Han,  
Lucas Silva, Jinwha Shin, Fortunat Joos, Jérôme Chappellaz, Hubertus  
Fischer, Thomas Stocker

### ► To cite this version:

Loïc Schmidely, Christoph Nehrbass-Ahles, Jochen Schmitt, Juhyeong Han, Lucas Silva, et al.. CH<sub>4</sub> and N<sub>2</sub>O fluctuations during the penultimate deglaciation. *Climate of the Past*, 2021, 17 (4), pp.1627-1643. 10.5194/cp-17-1627-2021 . hal-03418313

**HAL Id: hal-03418313**

**<https://hal.science/hal-03418313>**

Submitted on 7 Nov 2021

**HAL** is a multi-disciplinary open access archive for the deposit and dissemination of scientific research documents, whether they are published or not. The documents may come from teaching and research institutions in France or abroad, or from public or private research centers.

L'archive ouverte pluridisciplinaire **HAL**, est destinée au dépôt et à la diffusion de documents scientifiques de niveau recherche, publiés ou non, émanant des établissements d'enseignement et de recherche français ou étrangers, des laboratoires publics ou privés.



# CH<sub>4</sub> and N<sub>2</sub>O fluctuations during the penultimate deglaciation

Loïc Schmidely<sup>1</sup>, Christoph Nehrbass-Ahles<sup>2</sup>, Jochen Schmitt<sup>1</sup>, Juhyeong Han<sup>1</sup>, Lucas Silva<sup>1</sup>, Jinwha Shin<sup>3,a</sup>, Fortunat Joos<sup>1</sup>, Jérôme Chappellaz<sup>3</sup>, Hubertus Fischer<sup>1</sup>, and Thomas F. Stocker<sup>1</sup>

<sup>1</sup>Climate and Environmental Physics, Physics Institute and Oeschger Centre for Climate Change Research, University of Bern, Bern 3012, Switzerland

<sup>2</sup>Department of Earth Sciences, University of Cambridge, Cambridge, UK

<sup>3</sup>Institut des Géosciences de l'Environnement (IGE), CNRS, Univ. Grenoble-Alpes, Grenoble, France

<sup>a</sup>present address: Department of Earth and Atmospheric Sciences, University of Alberta, Edmonton, AB, T6G 2E3, Canada

**Correspondence:** Thomas F. Stocker (thomas.stocker@climate.unibe.ch)

Received: 30 September 2020 – Discussion started: 19 October 2020

Revised: 12 May 2021 – Accepted: 1 July 2021 – Published: 3 August 2021

**Abstract.** Deglaciations are characterized by the largest natural changes in methane (CH<sub>4</sub>) and nitrous oxide (N<sub>2</sub>O) concentrations of the past 800 000 years. Reconstructions of millennial- to centennial-scale variability within these periods are mostly restricted to the last deglaciation. In this study, we present composite records of CH<sub>4</sub> and N<sub>2</sub>O concentrations from the EPICA Dome C ice core covering the penultimate deglaciation at temporal resolutions of  $\sim 100$  years. Our data permit the identification of centennial-scale fluctuations during the transition from glacial to interglacial levels. At  $\sim 134$  000 and  $\sim 129$  000 years before present (hereafter ka), both CH<sub>4</sub> and N<sub>2</sub>O increased on centennial timescales. These abrupt rises are similar to the fluctuations associated with the Dansgaard–Oeschger events identified in the last glacial period. In addition, gradually rising N<sub>2</sub>O levels at  $\sim 130$  ka resemble a pattern of increasing N<sub>2</sub>O concentrations on millennial timescales characterizing the later part of Heinrich stadials. Overall, the events in CH<sub>4</sub> and N<sub>2</sub>O during the penultimate deglaciation exhibit modes of variability that are also found during the last deglaciation and glacial cycle, suggesting that the processes leading to changes in emission during the transitions were similar but their timing differed.

tive balance in the future depends on the sensitivity of natural sources to anthropogenic warming. Time periods of climate change in the past provide natural templates to study this coupling (Fischer et al., 2018). Reconstructions of greenhouse gas concentrations before the instrumental era are only enabled by analysing the composition of air trapped in tiny bubbles in polar ice cores, reflecting the atmospheric composition at the time the bubbles were formed. Ice core records of CH<sub>4</sub> and N<sub>2</sub>O concentrations combined with temperature reconstructions revealed the natural variability of these gases and their coupling to climate change during the glacial cycles of the past 800 000 years. The overall increase in concentrations accompanying deglaciations represents the largest recurring changes (Spahni et al., 2005; Loulergue et al., 2008; Schilt et al., 2010a). Records spanning the last deglaciation (Termination I (TI), 18 000–11 000 years before present (hereafter ka), where present is defined as 1950 Common Era) showed that this overall increase appears as a sequence of millennial and centennial fluctuations superimposed, for CH<sub>4</sub>, on longer-term, gradually rising concentrations (Marrcott et al., 2014; Rhodes et al., 2015). Records resolving short-term fluctuations within deglaciations are limited to TI, owing to the availability of multiple high-accumulation ice cores.

The aim of this study is to produce a high-resolution deglacial record for the penultimate deglaciation (Termination II (TII), 140–128 ka). We present CH<sub>4</sub> and N<sub>2</sub>O composite datasets from the EPICA Dome C (EDC) ice core including 150 new measurements covering the time interval 145–125 ka, combined with the published data of Loulergue et al.

## 1 Introduction

Methane (CH<sub>4</sub>) and nitrous oxide (N<sub>2</sub>O) are currently the second- and third-most potent well-mixed anthropogenic greenhouse gases after carbon dioxide (CO<sub>2</sub>) (Myhre et al., 2013). The impact of these trace gases on the Earth's radia-

(2008) and Schilt et al. (2010a). We increased the sampling resolution of the aforementioned records by a factor  $\sim 3.5$  and  $\sim 5$  to obtain mean resolutions of 100 and 115 years for CH<sub>4</sub> and N<sub>2</sub>O, respectively. These values are on the order of the mean width of the gas age distribution (GAD) for the EDC ice core in the interval 145–125 ka. This width is estimated to range between  $\sim 110$ –220 years using the approach of Nehrbass-Ahles et al. (2020), where the width is defined as the arithmetic mean of the distribution, and  $\sim 50$ –130 years using the approach of Epifanio et al. (2020), where the width is defined as the spectral width of the distribution. In addition, we also present seven N<sub>2</sub>O isotopic measurements ( $\delta^{15}\text{N}$  (N<sub>2</sub>O) and  $\delta^{18}\text{O}$  (N<sub>2</sub>O)), used to assess the integrity of the data with respect to in situ formation of N<sub>2</sub>O.

CH<sub>4</sub> and N<sub>2</sub>O fluctuations observed during TI belong to recurrent modes of variability. The most studied of these modes characterizes the climate transitions from stadials to interstadials and is most notably exemplified by the transitions associated with the Dansgaard–Oeschger (DO) events of the last glacial period as well as by the transitions to the Bølling–Allerød and the Holocene during TI. This *DO-type* mode of variability is characterized by abrupt increases in CH<sub>4</sub> concentrations ( $\sim 50$ –260 ppb in a few centuries), approximately synchronous with the onsets of interstadial Greenland warming by a few decades (Baumgartner et al., 2014; Rosen et al., 2014), while N<sub>2</sub>O concentrations exhibit concomitant increases reaching up to  $\sim 60$  ppb, taking more than a century to stabilize because of their longer atmospheric lifetime (Flückiger et al., 2004; Schilt et al., 2010a, 2013). In addition, N<sub>2</sub>O concentrations gradually increase in the later part of Heinrich stadials (HSs), extended stadials defined by the occurrence of massive iceberg discharges through the Hudson Strait into the North Atlantic (Hemming, 2004), starting centuries to millennia before interstadial Greenland temperature and CH<sub>4</sub> rises (Schilt et al., 2013). This *late HS-type* mode of N<sub>2</sub>O variability characterized the HS during both the last deglaciation (Fischer et al., 2019; Schilt et al., 2014) as well as the last glacial period (Schilt et al., 2013). A second mode of CH<sub>4</sub> variability has been identified during HSs of the last glacial and deglaciation. This *HS-type* mode of CH<sub>4</sub> variability consists of intermittent CH<sub>4</sub> peaks displaying amplitudes of 32–53 ppb and characteristic timescales of 90–190 years, sometimes followed (HS4 and HS5) by elevated background concentrations relative to before the event (Rhodes et al., 2015).

DO-type and HS-type CH<sub>4</sub> fluctuations are likely driven by changes in tropical wetland emissions (Rhodes et al., 2015; Bock et al., 2017), where CH<sub>4</sub> is produced by the decomposition of organic matter under anaerobic conditions. Changes in geologic and pyrogenic emissions as well as changes in the sink strength play only a minor role (Dyonisius et al., 2020; Bock et al., 2010, 2017; Levine et al., 2012; Hopcroft et al., 2017). Wetland emissions are controlled by climate (precipitation, temperature, and atmospheric CO<sub>2</sub> concentration), modulating wetland extent, emission rates,

and ecosystem composition (Van Groenigen et al., 2011; Melton et al., 2013; Bloom et al., 2010). Changes in tropical wetland emissions during DO-type fluctuations are linked to the strengthening of monsoonal precipitation in the Northern Hemisphere (NH) tropics, enhancing wetland emission rates (Bock et al., 2017). Increased NH tropical precipitation is associated with northward shifts of the Intertropical Convergence Zone (ITCZ) in response to changes in heat distribution by the Atlantic Meridional Overturning Circulation (AMOC) (Broccoli et al., 2006; Alley, 2007). On the other hand, HS-type CH<sub>4</sub> fluctuations are hypothesized to result from large iceberg discharges, associated with a southward shift of the ITCZ, leading to an intensification of monsoonal precipitation in the Southern Hemisphere (SH) tropics, ultimately producing an increase in wetland emissions (Rhodes et al., 2015).

DO-type N<sub>2</sub>O variability is likely driven by changes in emission from the terrestrial and marine biospheres, where N<sub>2</sub>O is emitted as a by-product of nitrification and an intermediate product of denitrification (Joos et al., 2019, 2020; Fischer et al., 2019; Schilt et al., 2014). Terrestrial emissions are controlled by climate (precipitation, temperature, and atmospheric CO<sub>2</sub> concentration) and available land area (Joos et al., 2020; Van Groenigen et al., 2011). During TI, the response of terrestrial N<sub>2</sub>O emissions for DO-type fluctuations is believed to result from temperature and precipitation changes (Joos et al., 2020) and appeared in phase with Greenland warming with the transition period lasting a maximum of  $\sim 200$  years (Fischer et al., 2019). Marine emissions are linked to the strength of the AMOC, modulating oxygen concentrations in the upper ocean and the amount of available organic matter at depth. For DO-type fluctuations, marine emissions are believed to be stimulated mainly by deoxygenation in the upper ocean as a consequence of the reinvigoration of the AMOC (Joos et al., 2019). Finally, the late HS-type N<sub>2</sub>O increase during TI is thought to be driven exclusively by marine emissions (Fischer et al., 2019; Schilt et al., 2014), possibly resulting from a long-term reorganization of the nitrate and oxygen inventories following the preceding AMOC collapse (Schmittner and Galbraith, 2008).

## 2 Method

The results presented in this study are derived from two different instruments. The  $\delta^{15}\text{N}$  (N<sub>2</sub>O) and  $\delta^{18}\text{O}$  (N<sub>2</sub>O) data were measured with the device described in Schmitt et al. (2014), combining continuous extraction under vacuum with gas chromatography (GC) and isotope ratio mass spectrometry.

CH<sub>4</sub> and N<sub>2</sub>O measurements were performed with a completely revised analytical system, firstly employed during this study (comprehensive description in Appendix A). The new apparatus uses continuous extraction under vacuum, comparable to the approach of Schmitt et al. (2014) or

Oyabu et al. (2020), combined with GC techniques to determine CH<sub>4</sub> and N<sub>2</sub>O mole fractions in air extracted from small (~ 20 g) ice samples with a sample throughput of five to six samples per day. The instrument is equipped with a thermal conductivity detector, a flame-ionization detector, and an electron-capture detector for the quantification of air, CH<sub>4</sub>, and N<sub>2</sub>O, respectively. The results are referenced to the World Meteorological Organisation mole fraction scales: the WMOX2004A scale (CH<sub>4</sub>) and NOAA-2006A (N<sub>2</sub>O) (Dlugokencky et al., 2005; Hall et al., 2007) using three standard gases bracketing the glacial–interglacial range of CH<sub>4</sub> ( $358.88 \pm 0.16$  ppb,  $838.59 \pm 0.28$  ppb, and  $1729.30 \pm 0.34$  ppb) and N<sub>2</sub>O concentrations ( $187.10 \pm 0.12$  ppb,  $194.13 \pm 0.12$  ppb, and  $300.20 \pm 0.12$  ppb). The uncertainty of the measurements derived from the revised instrument amounts to 7 (CH<sub>4</sub>) and 6 ppb (N<sub>2</sub>O).

### 3 Results

Our centennial-scale records show the progressions of the overall ~ 390 and ~ 60 ppb increase in CH<sub>4</sub> and N<sub>2</sub>O concentration (Fig. 1), respectively, from the end of the Penultimate Glacial Maximum (PGM) to the beginning of the Last Interglacial (LIG). Our CH<sub>4</sub> data identify an outstanding value at ~ 140 ka in the dataset by Louergue et al. (2008), ~ 80 ppb higher than adjacent samples (Fig. 1). The N<sub>2</sub>O data appear substantially more scattered in the early part of the record, especially around the PGM (~ 145–140 ka). This scatter tends to decrease with younger ages. The spikes appear in the interval where the isotopic composition of N<sub>2</sub>O becomes enriched in  $\delta^{15}\text{N}$  (N<sub>2</sub>O) (up to 21 ‰) and depleted in  $\delta^{18}\text{O}$  (N<sub>2</sub>O) (down to 41 ‰), compared to the relatively steady values in the ranges ~ 11–14 ‰ and ~ 45–47 ‰, respectively, observed for 125–136 ka (Fig. 1).

Our records display several fluctuations standing out in the overall evolution of the CH<sub>4</sub> and N<sub>2</sub>O concentrations. For CH<sub>4</sub>, these events are identified based on their high rates of change (> 10 ppb per century, Table 1). CH<sub>4</sub> rises on centennial timescales at ~ 134 and ~ 129 ka. At ~ 134 ka, concentrations increased by ~ 70 ppb in ~ 200 years before declining by ~ 60 ppb in ~ 400 years. The 129 ka event consists of a ~ 200 ppb increase proceeding in ~ 300 years.

The evolution of N<sub>2</sub>O concentrations alternates between periods of plateaus and well-marked fluctuations. Similar to CH<sub>4</sub>, a feature is resolved at ~ 134 ka where concentrations increased by ~ 30 ppb in ~ 300 years before declining to previous levels in ~ 1000 years. The 129 ka event is also imprinted in our N<sub>2</sub>O record and is characterized by a ~ 30 ppb rise in ~ 900 years. In addition, an increase is identified at ~ 130 ka, where concentrations rose by ~ 20 ppb in ~ 700 years. The 130 and 129 ka events are separated by a plateau that lasted ~ 1000 years.

Overall, the improved resolution of our records allowed us to identify features not resolved in the previously published CH<sub>4</sub> and N<sub>2</sub>O EDC datasets. In particular, the 134 ka event and the 130 ka event in N<sub>2</sub>O are resolved for the first time. Retrieving CH<sub>4</sub> and N<sub>2</sub>O concentrations from the same samples enables us to study the relative phasing of both trace gases in the course of these events without age uncertainty. At the onset of the 134 and 129 ka events, the rise in both trace gases occurs simultaneously. In contrast, the 130 ka event in the N<sub>2</sub>O record is not accompanied by a concomitant fluctuation in CH<sub>4</sub> concentrations.

## 4 Discussion

### 4.1 Non-atmospheric CH<sub>4</sub> and N<sub>2</sub>O variability

Interpreting our records in terms of atmospheric variability requires a closer inspection of the extreme values observed in the CH<sub>4</sub> and N<sub>2</sub>O records.

The CH<sub>4</sub> data point at ~ 140 ka, previously published by Louergue et al. (2008), is measured in the section characterized by the widest GAD in our record. For the time interval 141–139 ka, the width of the GAD is on the order of ~ 220 years, using the approach of Nehrbass-Ahles et al. (2020), or ~ 120 years using the approach of Epifanio et al. (2020). At ~ 140 ka, the adjacent data points are ~ 160 years older and ~ 170 years younger than the data point in question. Consequently, it appears unlikely that such an abrupt fluctuation in the ice core record represents an atmospheric signal. Spurious peaks could potentially result from layered bubble trapping (Rhodes et al., 2016; Fourteau et al., 2017, 2020). However, this outlier is measured in a period of otherwise stable CH<sub>4</sub> concentrations, where neither early nor late pore closures are expected to generate an anomaly (Rhodes et al., 2016; Fourteau et al., 2017). Secondly, similarly high concentrations are not observed in our record before the 134 ka event. Such an age anomaly (between the layers enclosing gas of abnormal age and the layers enclosing gas of the expected age) would be unrealistically high compared to the characteristic age anomalies reported by Fourteau et al. (2017) for the Vostok ice core (~ 200 years). Accordingly, we regard this CH<sub>4</sub> data point as an outlier.

The large variability observed in adjacent data points during the early part of the N<sub>2</sub>O record (Fig. 1) is unlikely to reflect atmospheric fluctuations given its atmospheric lifetime of  $116 \pm 9$  years (Prather et al., 2015). Elevated concentrations and disproportionately high N<sub>2</sub>O variability have been observed in many instances for ice samples rich in mineral dust in both Antarctic and Greenland ice cores and are attributed to in situ production (Flückiger et al., 1999; Sowers, 2001; Flückiger et al., 2004; Spahni et al., 2005; Schilt et al., 2010a, 2013; Fischer et al., 2019). Measurements in the Vostok ice core by Sowers (2001) demonstrated this excess N<sub>2</sub>O production to have a strong imprint in both  $\delta^{15}\text{N}$  (N<sub>2</sub>O) and  $\delta^{18}\text{O}$  (N<sub>2</sub>O) records. For some of our EDC samples we ob-

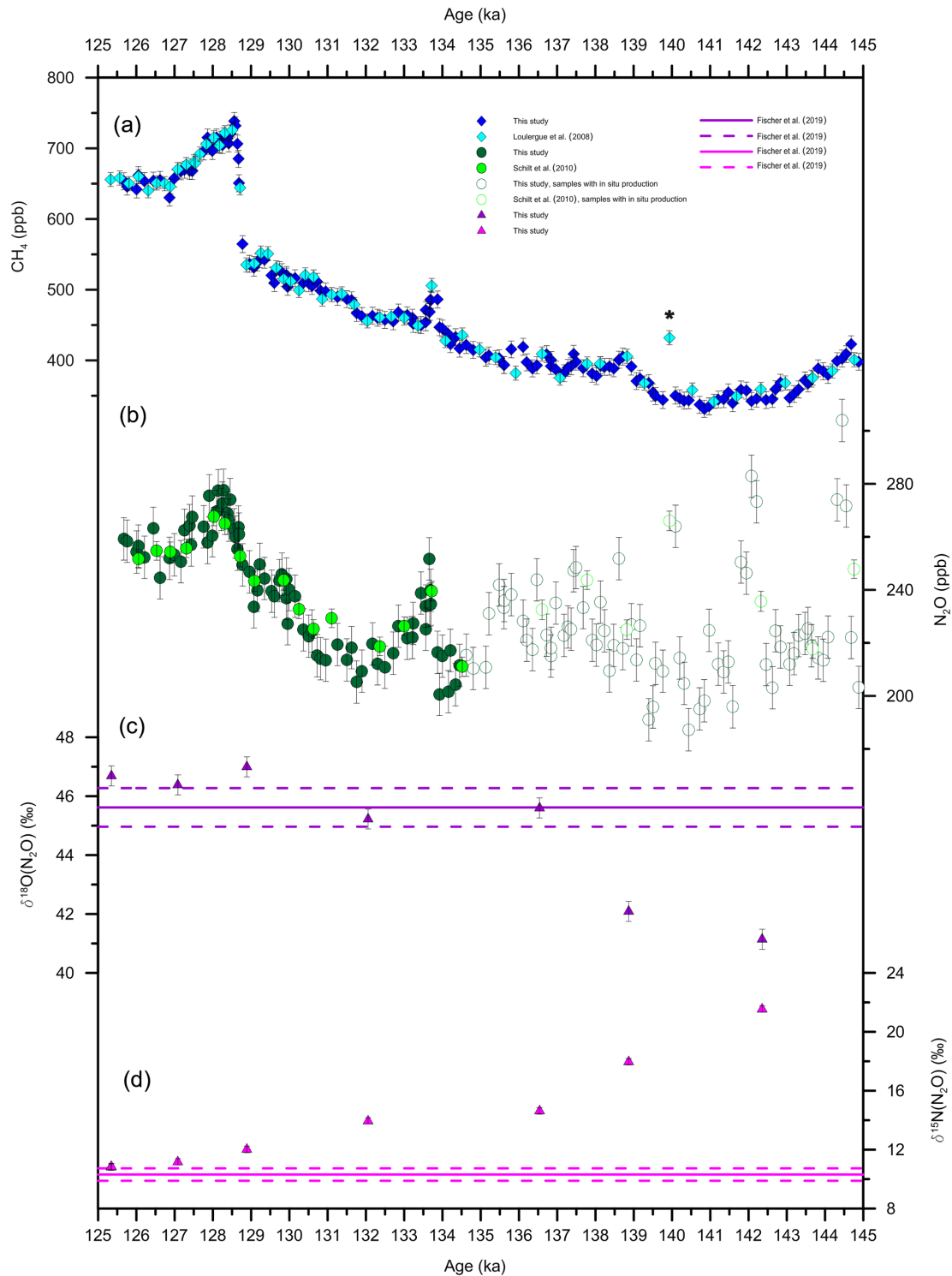


**Figure 1.** CH<sub>4</sub>, N<sub>2</sub>O, δ<sup>18</sup>O (N<sub>2</sub>O), and δ<sup>15</sup>N (N<sub>2</sub>O) records from the EDC ice core on the AICC2012 timescale (Bazin et al., 2013). The vertical bars represent the uncertainty of the measurements. **(a)** Composite CH<sub>4</sub> record with published data (light blue, Louergue et al., 2008) and new measurements (this study, dark blue) after offset correction. The asterisk indicates the data point regarded as an outlier. **(b)** Composite N<sub>2</sub>O record with published data (light green, Schilt et al., 2010a) and new measurements (this study, dark green) after offset correction. The empty symbols illustrate the data points considered affected by in situ production. **(c)** δ<sup>18</sup>O (N<sub>2</sub>O) record. For comparison, the average (solid line) and standard deviation (dashed line, 1σ) of δ<sup>18</sup>O (N<sub>2</sub>O) over TI are included (Fischer et al., 2019). **(d)** δ<sup>15</sup>N (N<sub>2</sub>O) record. For comparison, the average (solid line) and standard deviation (dashed line, 1σ) of δ<sup>15</sup>N (N<sub>2</sub>O) over TI are included (Fischer et al., 2019).



**Table 1.** Characteristics of the events observed at  $\sim 134$ ,  $\sim 129$ , and  $\sim 130$  ka. The indications “up” and “down” in the first column refer to the ascending and descending limbs of the 134 ka event, respectively. The columns “start” and “end” indicate the starting and end points of the events (rounded to the hundred). The columns  $C_{\text{initial}}$  and  $C_{\text{final}}$  indicate the concentrations (rounded to the 10) in the years preceding and following the events, respectively. The rates of change are average values over the time period comprised between the start and end points of the events. Rates of change are calculated from spline approximations (cut-off period: 200 years) computed according to Enting (1987) with the same routine as Beck et al. (2018).

Event	Start (ka)	End (ka)	$C_{\text{initial}}$ (ppb)	$C_{\text{final}}$ (ppb)	Rate of change (ppb per century)
134 (CH <sub>4</sub> , up)	134.0	133.8	440	510	35
134 (CH <sub>4</sub> , down)	133.8	133.4	510	450	−15
134 (N <sub>2</sub> O, up)	133.9	133.6	210	240	10
134 (N <sub>2</sub> O, down)	133.6	132.6	240	210	−3
130 (N <sub>2</sub> O)	130.7	130	220	240	3
129 (CH <sub>4</sub> )	128.9	128.6	530	730	65
129 (N <sub>2</sub> O)	129	128.1	240	270	3

serve the same systematic isotopic deviations as for the Vostok samples of that period, with  $\delta^{15}\text{N}$  (N<sub>2</sub>O) and  $\delta^{18}\text{O}$  (N<sub>2</sub>O) values that are more enriched and depleted, respectively, than typical atmospheric values. The coupling with dust is the basis of an empirical artefact detection method applicable to EDC samples. This method considers depth intervals where dust concentrations exceed an arbitrary threshold of  $300\text{ }\mu\text{g kg}^{-1}$  as affected by in situ production (Spahni et al., 2005; Schilt et al., 2010a). We follow this approach and define 134.5 ka as the boundary for the section affected by artefacts. This is a slightly younger age than the last value regarded as unbiased by Schilt et al. (2010a). Consequently, we refrain from interpreting N<sub>2</sub>O data points older than 134.5 ka as reflecting atmospheric variability.

The younger part of our records are used to study CH<sub>4</sub> and N<sub>2</sub>O fluctuations during TII. In particular, we scrutinize our record with respect to the newly resolved variations belonging to the modes of variability presented above. To achieve this, we analyse the characteristics of the individual events as well as the background climate in which they occur.

#### 4.2 The 129 ka event

The 129 ka event refers to the pronounced increase in CH<sub>4</sub> and N<sub>2</sub>O concentrations to interglacial levels at the end of TII (Fig. 2). For both gases, this event accounts for about half of the deglacial change in concentrations.

CH<sub>4</sub> and N<sub>2</sub>O concentrations rose in parallel with the main resumption of the AMOC, as indicated by the evolution of the isotopic ratio of neodymium 143 and 144 ( $\epsilon_{\text{Nd}}$ ) (Deaney et al., 2017; Böhm et al., 2015). At the same time, the evolution of the isotopic composition of speleothem calcite ( $\delta^{18}\text{O}$  (CaCO<sub>3</sub>)) indicates a northward shift of the ITCZ (Cheng et al., 2009, 2016) (Fig. 3). These are fingerprints of DO-type variability. Accordingly, the abrupt CH<sub>4</sub> rise likely reflects the response of terrestrial emissions from NH tropical wetlands. The simultaneous increase in both gases in-

dicates that terrestrial emissions contributed, at least partly, to the N<sub>2</sub>O rise at  $\sim 129$  ka. However, because the deglacial AMOC resumption occurred at this time, it can be assumed that marine sources also played a role. A contribution from both marine and terrestrial emissions is in agreement with the findings of Schilt et al. (2014) and Fischer et al. (2019) for DO-type fluctuations during TI. Higher resolution measurements of the isotopic composition of N<sub>2</sub>O combined with a deconvolution, similar to the aforementioned studies, are needed to quantitatively determine the relative contribution of the sources during the 129 ka event.

#### 4.3 The 130 ka event

The 129 ka event is preceded by a phase of rising N<sub>2</sub>O concentrations in the interval from 130.7 to 130 ka at the end of HS11 (Fig. 2). This is reminiscent of the pattern of late HS-type increase, where N<sub>2</sub>O concentrations rose before the rapid DO-type Greenland temperature and CH<sub>4</sub> increases (Schilt et al., 2013). The timescale of the 130 ka event is in the range of the duration typically observed for these episodes ( $\sim 0.5$ – $2$  millennia) (Schilt et al., 2013), while the N<sub>2</sub>O growth rate appears slightly larger ( $\sim 3$  ppb compared to typically  $\sim 1$  ppb per century). The lack of a concomitant CH<sub>4</sub> fluctuation suggests that only the marine source contributed to the N<sub>2</sub>O increase, in agreement with the findings of Schilt et al. (2014) and Fischer et al. (2019) for the late HS1 rise. The change in marine emissions may be linked to a long-term adjustment of the nitrate and oxygen inventories in the upper ocean after a period of AMOC interruption (Schmittner and Galbraith, 2008). Overall, despite the somewhat different rates of change, the 130 ka event likely constitutes an instance of a late-HS N<sub>2</sub>O fluctuation during TII. The attribution of the 130 ka feature to the pattern of late HS increase would be strengthened by additional measurements of  $\delta^{15}\text{N}$  (N<sub>2</sub>O) and  $\delta^{18}\text{O}$  (N<sub>2</sub>O), allowing the unambiguous identification of the source contributing to this event.

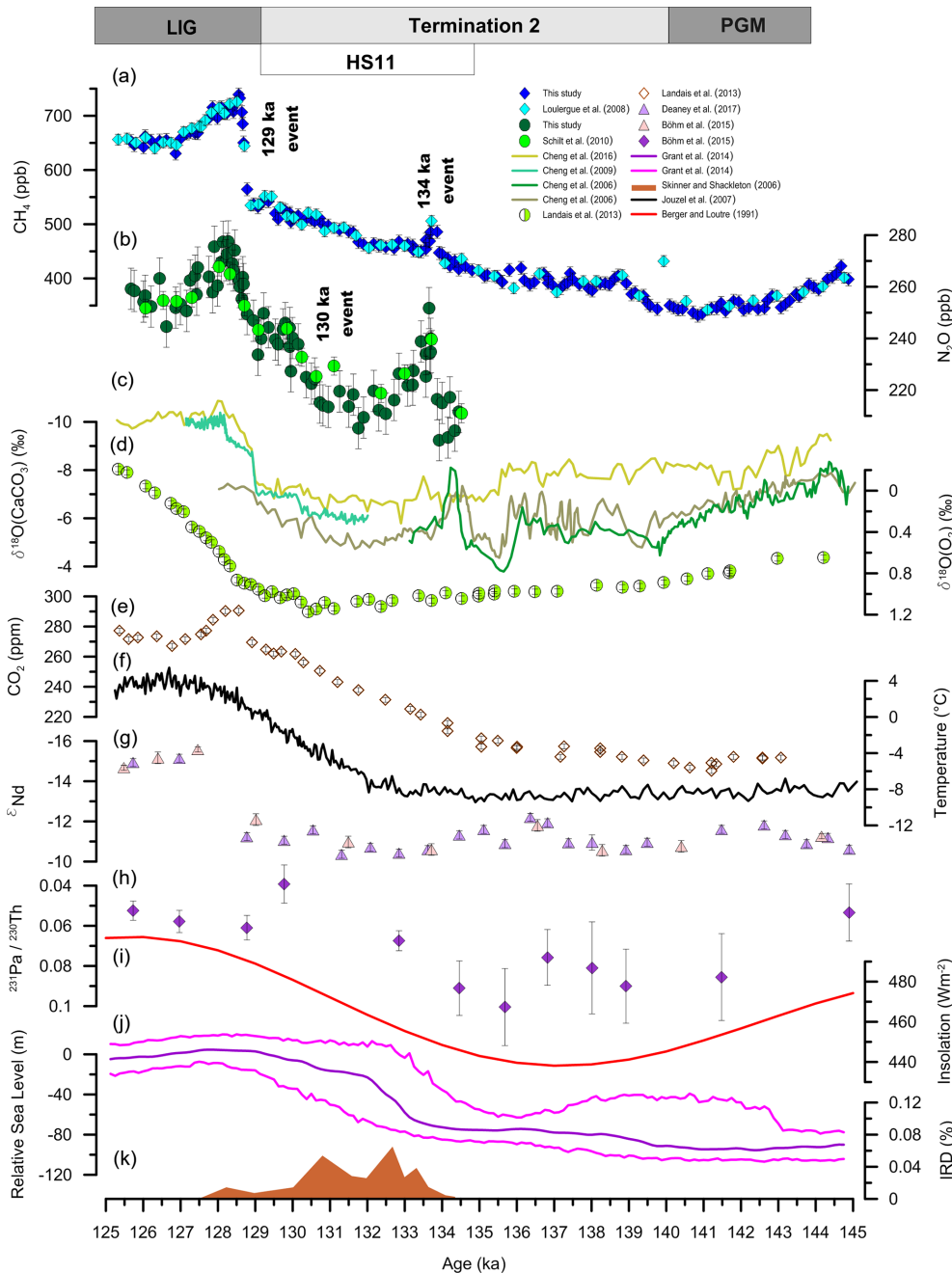


**Figure 2.** Evolution of the CH<sub>4</sub> and N<sub>2</sub>O concentrations combined with complementary climate proxies during TII. The boxes delineate the climate periods mentioned in the text: the Penultimate Glacial Maximum (PGM), Heinrich Stadial 11 (HS11, delineation according to Marino et al., 2015), and the Last Interglacial (LIG). (a) Composite CH<sub>4</sub> record. (b) Composite N<sub>2</sub>O record. (c) Speleothem  $\delta^{18}\text{O}$  (CaCO<sub>3</sub>) records: Sanbao SB25 (light green) (Cheng et al., 2009), Hulu Cave MSX (khaki) (Cheng et al., 2006), Hulu cave MSP (dark green) (Cheng et al., 2006), and Sanbao–Dongge composite (pale yellow) (Cheng et al., 2016). (d)  $\delta^{18}\text{O}$  (O<sub>2</sub>) from EDC on the AICC2012 timescale (Landais et al., 2013). (e) CO<sub>2</sub> from EDC on the AICC2012 timescale (Landais et al., 2013). (f) Antarctic surface temperature (relative to the last millennium) from EDC on the AICC2012 timescale (Jouzel et al., 2007). (g) Composite  $\epsilon_{\text{Nd}}$  from the sediment core ODP Site 1063 (Deaney et al., 2017), including data points from Böhm et al. (2015) (purple) and new measurements from Deaney et al. (2017) (pale pink), on the timescale of Deaney et al. (2017). (h)  $^{231}\text{Pa}/^{230}\text{Th}$  record from the sediment core ODP Site 1063 (Böhm et al., 2015), on the timescale of Deaney et al. (2017). (i) Mean summer (June to August) insolation at 40° N (Berger and Loutre, 1991). (j) Relative sea level stand from the Red Sea synchronized on a radiometric timescale, including the maximum probability curve (purple) and its 95 % confidence interval (magenta) (Grant et al., 2014). (k) Ice-rafted debris (IRD) from Skinner and Shackleton (2006) on the radiometric timescale of Marino et al. (2015).

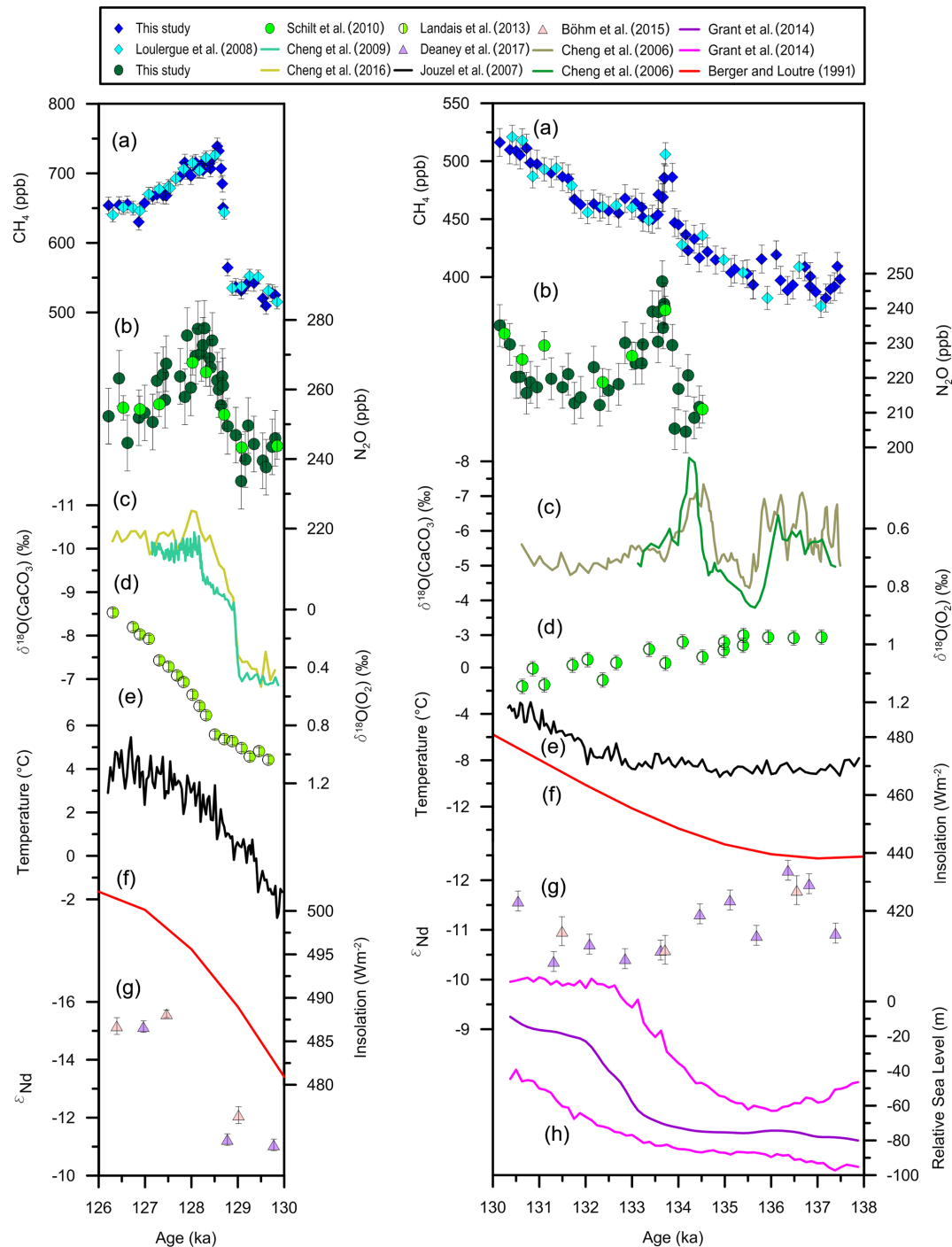


**Figure 3.** Details of the 129 (left panel) and 134 ka events (right panel). (a) Composite CH<sub>4</sub> record. (b) Composite N<sub>2</sub>O record. (c) Speleothem  $\delta^{18}\text{O}(\text{CaCO}_3)$  records: Sanbao SB25 (light green) (Cheng et al., 2009), Hulu Cave MSX (khaki) (Cheng et al., 2006), and Sanbao–Dongge composite (pale yellow). (d)  $\delta^{18}\text{O}(\text{O}_2)$  from EDC on the AICC2012 timescale (Landais et al., 2013). (e) Antarctic surface temperature (relative to the last millennium) from EDC on the AICC2012 timescale (Jouzel et al., 2007). (f) Mean summer (June to August) insolation at 40° N (Berger and Loutre, 1991). (g) Composite  $\epsilon_{\text{Nd}}$  from the sediment core ODP Site 1063 (Deaney et al., 2017), including data points from Böhm et al. (2015) (purple) and new measurements from Deaney et al. (2017) (pale pink), on the timescale of Deaney et al. (2017). (h) Relative sea level stand from the Red Sea synchronized on a radiometric timescale, including the maximum probability curve (purple) and its 95 % confidence interval (magenta) (Grant et al., 2014).



#### 4.4 The 134 ka event

Turning to the 134 ka event, its occurrence within HS11 and the properties of the CH<sub>4</sub> increase (duration and amplitude) are reminiscent of the HS-type pattern of variability evidenced by Rhodes et al. (2015). HS-type fluctuations resolved in the WAIS Divide (WD) ice core fully developed within 90–190 years (Rhodes et al., 2015). The broader GAD of the EDC ice core implies that any such features would appear strongly dampened in our data. This is supported by continuous CH<sub>4</sub> measurements in the Vostok ice core, demonstrating the absence of the characteristic overshoot resolved in the WD ice core during HS4 (Fourteau et al., 2020; Rhodes et al., 2015). Therefore, the sharpness and amplitude of the 134 ka event is not consistent with the picture of a substantially smoothed version of an HS-type fluctuation. The  $\sim 70$  ppb rise observed in the EDC record would translate into a WD signal exceeding by far the amplitude range of the HS1, HS2, HS4, and HS5 fluctuations (32–53 ppb) (Rhodes et al., 2015). Secondly, HS-type CH<sub>4</sub> variability is also characterized by abrupt CO<sub>2</sub> jumps, millennial-scale increases in  $\delta^{18}\text{O}$  (O<sub>2</sub>), enrichment in speleothem  $\delta^{18}\text{O}$  (CaCO<sub>3</sub>), and the absence of concomitant N<sub>2</sub>O variability (Bauska et al., 2016, 2018, 2021; Marcott et al., 2014; Fischer et al., 2019; Schilt et al., 2013, 2010a; Guillevic et al., 2014). The simultaneous occurrence of the CH<sub>4</sub> and N<sub>2</sub>O pulses at  $\sim 134$  ka, the depletion in speleothem  $\delta^{18}\text{O}$  (CaCO<sub>3</sub>), and the lack of any fluctuation in the  $\delta^{18}\text{O}$  (O<sub>2</sub>) record (Landais et al., 2013) contradict these observations (Fig. 3). The 134 ka event is therefore likely to have resulted from different mechanisms and does not constitute an instance of an HS-type CH<sub>4</sub> fluctuation during TII. On the other hand, simultaneous rises of atmospheric CH<sub>4</sub> and N<sub>2</sub>O concentrations are observed during DO-type fluctuations. During the last glacial cycle, the amplitude of DO-type CH<sub>4</sub> increases ranges from  $\sim 50$  to 220 ppb in Greenland ice cores and elevated concentrations lasted for centuries to millennia (Baumgartner et al., 2014; Flückiger et al., 2004). Accordingly, the magnitude of the 134 ka event fits well within the amplitude range observed for the well-resolved DO-type fluctuations in the EDC record of Loulergue et al. (2008) ( $\sim 50$ –185 ppb). Going further, results from Greenland ice cores have shown that the amplitude of DO-type CH<sub>4</sub> rises tracks the variations in low- to mid-latitude NH summer insolation, where the most substantial changes in concentration are associated with higher insolation. This indicates that the amount or seasonal distribution of solar radiation has modulated the response of CH<sub>4</sub> sources during interstadials (Brook et al., 1996; Flückiger et al., 2004). The 134 ka event occurs during a time period of low NH summer insolation (Fig. 2), comparable to this at DO2. Yet, the magnitude of the 134 ka event appears larger ( $\sim 70$  ppb compared to  $\sim 50$  ppb for DO2 in the EDC record).

Associating our event with a DO-type pattern of variability requires evidence for a northward shift of the ITCZ and rein-

vigoration of the AMOC. Synchronous with the 134 ka event, within dating uncertainty, we observe a short-lived negative excursion in speleothem  $\delta^{18}\text{O}$  (CaCO<sub>3</sub>) records (Cheng et al., 2006) (Fig. 3) as well as fluctuations in proxies reflecting salinity and runoff intensity in the Bay of Bengal (Nilsson-Kerr et al., 2019). These data indicate a transient strengthening of the NH tropical monsoon systems consistent with a northward shift of the ITCZ. Concerning the behaviour of the AMOC, we are not aware of studies reporting on a potential reinvigoration at this time. Nevertheless, oceanic tracers exhibit a small and short-lived fluctuation in the time interval 133–132 ka (on the timescale of Böhm et al., 2015) before reaching their maximum HS11 values (Böhm et al., 2015). On the updated chronology of the sediment core ODP Site 1063 (Deaney et al., 2017), the negative excursion in the  $\varepsilon_{\text{Nd}}$  record of Böhm et al. (2015) coincides with a comparably small value in the data of Deaney et al. (2017) (Fig. 2). However, the revised chronology places the excursion in  $\varepsilon_{\text{Nd}}$  and  $^{231}\text{Pa}/^{230}\text{Th}$  substantially earlier than the 134 ka event (Fig. 3). The onset of this excursion is at  $\sim 137.4$  ka, corresponding to a shift by  $\sim 4900$  years with respect to the timescale of Böhm et al. (2015). Since the timescale of the sediment core is tuned to the Antarctic Ice Core Chronology (AICC2012) (Bazin et al., 2013; Veres et al., 2013) within an estimated uncertainty of 400 years, the fluctuations resolved in the ice and marine cores should, in principle, not be regarded as synchronous. However, the alignment with the AICC2012 is performed using only one tie point between CH<sub>4</sub> and the isotopic composition of planktonic foraminifera (at  $\sim 128.7$  ka, corresponding to the abrupt CH<sub>4</sub> increase into the LIG) (Deaney et al., 2017). Therefore, it may be possible that the two timescales are less tightly aligned away from this tie point. If this would be the case, it could be hypothesized that the excursions in oceanic proxies are synchronous with the fluctuations of  $\delta^{18}\text{O}$  (CaCO<sub>3</sub>), CH<sub>4</sub>, and N<sub>2</sub>O.

DO-type variability is typically also imprinted in the temperature record from Antarctic ice cores as well as in the  $\delta^{18}\text{O}$  (O<sub>2</sub>) record. However, the responses of these proxies are generally attenuated or occur on longer timescales compared to those of CH<sub>4</sub> and  $\delta^{18}\text{O}$  (CaCO<sub>3</sub>). Accordingly, a short and small-amplitude interstadial at  $\sim 134$  ka might not have left discernible imprints in the respective records of Landais et al. (2013) and Jouzel et al. (2007) (Figs. 2 and 3).

Taking the proxy evidences together, we speculate that a brief and small-scale resumption of the AMOC might have occurred within HS11, accounting for the northward ITCZ shift and the rise in atmospheric CH<sub>4</sub> and N<sub>2</sub>O concentrations. We acknowledge that our interpretation is limited by the relatively coarse resolution of  $\varepsilon_{\text{Nd}}$  and  $^{231}\text{Pa}/^{230}\text{Th}$  as well as by the uncertainty arising from cross-dating sediment and ice core records. Concerning N<sub>2</sub>O, we finally note that the duration of the rise and the simultaneity with the excursion in CH<sub>4</sub> suggest that terrestrial N<sub>2</sub>O emissions con-

tributed by far the most to the 134 ka event (Fischer et al., 2019).

Should our interpretation hold, the 134 ka event can be regarded as a short DO-type fluctuation. We speculate that the hypothesized AMOC reinvigoration might have been perturbed by Meltwater Pulse 2B (MWP-2B). MWP-2B represents  $\sim 70\%$  of the deglacial sea level change and coincides with the 134 ka event within dating uncertainty (Fig. 2) (Marino et al., 2015). The disruption of the oceanic circulation by freshwater forcing might have been enabled by the high susceptibility of the AMOC to perturbations at a time when the high-latitude SH was particularly cold (Buizert and Schmittner, 2015), as was the case during HS11 (Fig. 2). This situation favours the occurrence of relatively short, centennial, interstadials such as those appearing near the Last Glacial Maximum in Greenland ice cores.

## 5 Conclusions

In the present study, we increased the resolution of the deglacial CH<sub>4</sub> and N<sub>2</sub>O records, allowing us to derive composite datasets covering TII (140–128 ka) at average resolutions of  $\sim 100$  years. Our results display pronounced fluctuations standing out of the overall transition of CH<sub>4</sub> and N<sub>2</sub>O concentrations to interglacial conditions. The most prominent one is placed at  $\sim 129$  ka and delineates the transition into the LIG. We assume that terrestrial and marine sources contributed to the N<sub>2</sub>O increase at this time. Additionally, we unequivocally identify a 134 and 130 ka event. We link the latter to the pattern of late HS-type N<sub>2</sub>O increase, where changes in marine emissions are likely to be the only contributor. The former is regarded as a short DO-type fluctuation, whose timescale indicates that only terrestrial N<sub>2</sub>O sources likely contributed to the increase. We note that these fluctuations in CH<sub>4</sub> and N<sub>2</sub>O concentrations during the penultimate deglaciation are all instances of recurrent modes of variability, also evidenced during the last deglaciation as well as during the last glacial period.

## Appendix A: New measurement system for CH<sub>4</sub> and N<sub>2</sub>O

Although gas chromatography (GC) has been used extensively to measure CH<sub>4</sub> and N<sub>2</sub>O at the University of Bern (e.g. Flückiger et al., 1999, 2002, 2004; Baumgartner et al., 2012, 2014; Loulergue et al., 2008; Schilt et al., 2010a, b, 2013; Spahni et al., 2005), the totally revised extraction and GC setup presented here has not been described before. The device is composed of different functional units, enabling the different actions of the system (standard injection, extraction, separation, and detection) (coloured boxes in Fig. A1). The measurements are carried out using three distinct lines. The ice line (IL, under vacuum, red path in Fig. A1) is used to extract air from ice core samples. The continuous-flow line (CFL, flushed with He, green path in Fig. A1) is used to measure standards to calibrate ice core measurements. Standards and samples are introduced differently into the separation unit to gain time during daily operation. Therefore, following the identical treatment principle, we also employ the standard over ice line (SOIL, blue line in Fig. A1) to periodically inject standards for comparison with similar measurements performed with the CFL in order to account for contamination stemming from the IL. The mean offset between the lines is used to correct IL data.

To extract gas from ice core samples, we use continuous extraction under vacuum. Air is released from the ice during the melting (immersing the bottom of the vessel in a  $\sim 20^\circ\text{C}$  water bath) and is simultaneously adsorbed on an activated charcoal trap held at  $-196^\circ\text{C}$  using liquid nitrogen (T2 in Fig. A1). Water vapour is condensed beforehand using another cold trap held at  $-80^\circ\text{C}$  (T1 in Fig. A1). The progression of the extraction is monitored with a pressure gauge (P5 in Fig. A1). The completion of the extraction is indicated by a P5 pressure value  $\leq 0.25$  mbar. When this value is reached, T2 is isolated from the vessel and heated to facilitate CH<sub>4</sub> and N<sub>2</sub>O desorption from the charcoal bed. The duration and final temperature of the heating (5 min,  $130^\circ\text{C}$ ) ensure full recovery of the adsorbed gas. At the end of this phase, He flushes the content of T2 into the separation unit. Overall, the advantage of our procedure is the permanently low CH<sub>4</sub> and N<sub>2</sub>O partial pressure, as well as total air pressure, prevailing in the vessel during the extraction. Accordingly, equilibrium conditions with respect to solubility are never reached, precluding the need of a solubility correction. This type of correction was required in traditional analyses using a melt–refreeze method, where the air sample is enclosed in the vessel head space during the extraction.

CH<sub>4</sub> and N<sub>2</sub>O are separated from the bulk air in the separation unit before reaching the detection unit equipped with a thermal conductivity detector (TCD), a flame-ionization detector (FID), and an electron-capture detector (ECD) to quantify the amount of air, CH<sub>4</sub>, and N<sub>2</sub>O, respectively. The separation unit is composed of a succession of GC columns. CH<sub>4</sub> and N<sub>2</sub>O are separated from the bulk air in the precol-

umn and analytical column (Fig. A1). After detection of the air peak by the TCD, V8 allows us to route CH<sub>4</sub> towards the FID (via T5 and T7) and N<sub>2</sub>O towards the ECD (via T4 and T6) (Fig. A1). T5 and T4 are used to separate CH<sub>4</sub> and N<sub>2</sub>O, respectively, from species having almost similar retention times. T7 and T6 are used to focus the gas to obtain sharp peaks in the chromatograph.

The amount of air, CH<sub>4</sub>, and N<sub>2</sub>O is quantified by integrating the area below the corresponding GC peaks. For each species, calibration curves are established between areas and the number of moles calculated using the volume, temperature, and pressure of the sample loop as well as the known CH<sub>4</sub> and N<sub>2</sub>O mole fractions of the standard gases. We use a set of primary standards provided by the National Oceanic and Atmospheric Administration and referenced to the World Meteorological Organisation mole fraction scales: the WMOX2004A scale (CH<sub>4</sub>) and NOAA-2006A (N<sub>2</sub>O) (Dlugokencky et al., 2005; Hall et al., 2007). This set of standards brackets the glacial–interglacial range of CH<sub>4</sub> ( $358.88 \pm 0.16$  ppb,  $838.59 \pm 0.28$  ppb, and  $1729.30 \pm 0.34$  ppb) and N<sub>2</sub>O concentrations ( $187.10 \pm 0.12$  ppb,  $194.13 \pm 0.12$  ppb, and  $300.20 \pm 0.12$  ppb). CH<sub>4</sub> and N<sub>2</sub>O mole fractions are calculated by dividing the number of CH<sub>4</sub> and N<sub>2</sub>O moles by the number moles of air. In addition, total air content can also be quantified using the TCD area as well as the volume, temperature, and pressure of the sample loop.

After calibration, the results are corrected for the line offset between CFL and SOIL. This offset accounts for the blank introduced in the IL and is averaged over, at least, a measurement campaign. The CH<sub>4</sub> and N<sub>2</sub>O line offsets appear to be linearly dependent on the concentration enabling the use of linear interpolations to correct ice core results.

The uncertainty of the CH<sub>4</sub> and N<sub>2</sub>O data derived with our instrument amounts to 7 and 6 ppb, respectively. It is calculated as the sum of the individual uncertainty, associated with the overall analytical procedure ( $1\sigma$  standard deviation of SOIL measurements) and with the line offset correction, in quadrature.

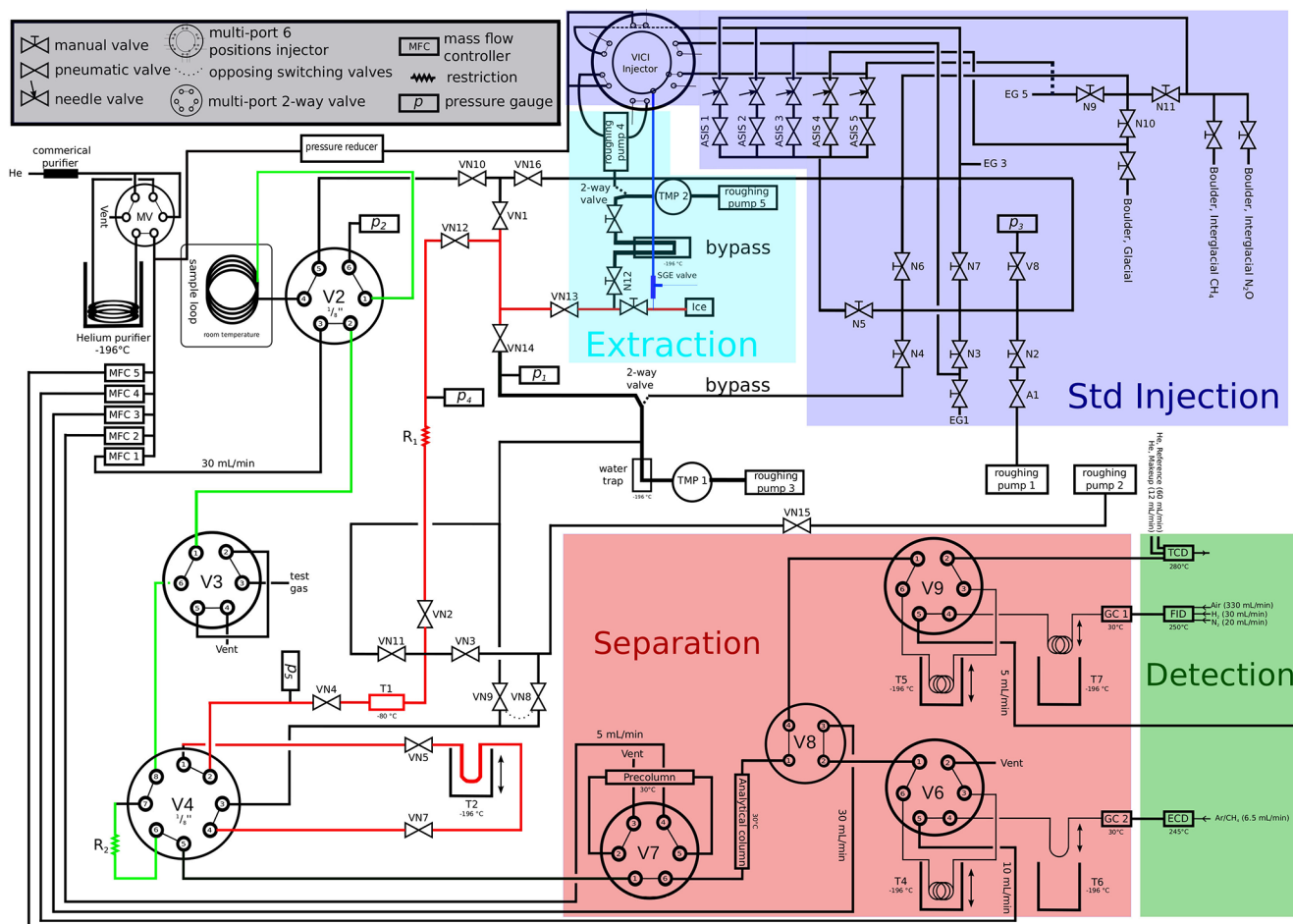


**Figure A1.** Flow scheme of the CH<sub>4</sub> and N<sub>2</sub>O measurement system. The red, green, and blue paths highlight the ice line (IL), continuous-flow line (CFL), and standard over ice line (SOIL), respectively. Coloured boxes display the different functional units of the system discussed in Appendix A.

## Appendix B: Construction of composite CH<sub>4</sub> and N<sub>2</sub>O records

The construction of the composite records presented in this study is complicated by offsets between the datasets, where our results appear on average  $18 \pm 10$  ppb (CH<sub>4</sub>) and  $21 \pm 3$  ppb (N<sub>2</sub>O) higher than previous data, although all datasets show the same relative changes (Fig. B1). The offsets are calculated as the mean of the residuals between splines with cut-off periods of 10 000 years fitted through the datasets. We computed splines according to Enting (1987), using the same routine as Beck et al. (2018), where each spline is the average of 1000 iterations with data points varied within a normal distribution inside their uncertainty range.

It seems likely that the offsets are linked to the different extraction techniques employed. In fact, the published EDC data were measured at the University of Bern and Grenoble with instruments using melt–refreeze extraction (Louergue et al., 2008; Schilt et al., 2010a). Melt–refreeze extraction is prone to underestimate CH<sub>4</sub> and N<sub>2</sub>O concentrations if the refreezing is not perfectly efficient, while in our method air is quantitatively extracted from the ice samples. We note that also the values presented in previous publications had to be aligned for interlaboratory offsets on the order of 10 ppb for CH<sub>4</sub> (Louergue et al., 2008), which may also reflect differences in the extraction efficiency of previously used melt–refreeze methods in different labs. Because melt–refreeze extraction has been the standard procedure for decades, the EDC records have been measured exclusively using this technique. We therefore think that additional overlapping measurements with an independent extraction technique (e.g. sublimation) are needed to resolve the dispute. Without further evidence, we prefer striving for consistency by correcting our data to the EDC benchmark records of Louergue et al. (2008) and Schilt et al. (2010a). To achieve this, we subtract the mean offsets of 18 (CH<sub>4</sub>) and 21 ppb (N<sub>2</sub>O) from our results. This approach is facilitated by the high degree of co-variation between the datasets (Fig. B1).

The merging procedure described above adds an additional source of uncertainty to our results. Accounting for the uncertainty of the mean offset, taken as the standard deviation ( $1\sigma$ ) of the residuals between the splines, increases the total uncertainty of the new data included in the composite records to 12 (CH<sub>4</sub>) and 8 ppb (N<sub>2</sub>O). For the published EDC values and the isotopic measurements, the uncertainties amount to 10 ppb (CH<sub>4</sub>), 4 ppb (N<sub>2</sub>O), 0.22 ‰ ( $\delta^{15}\text{N}$  (N<sub>2</sub>O)), and 0.34 ‰ ( $\delta^{18}\text{O}$  (N<sub>2</sub>O)), as reported in Louergue et al. (2008), Schilt et al. (2010a), and Schmitt et al. (2014).



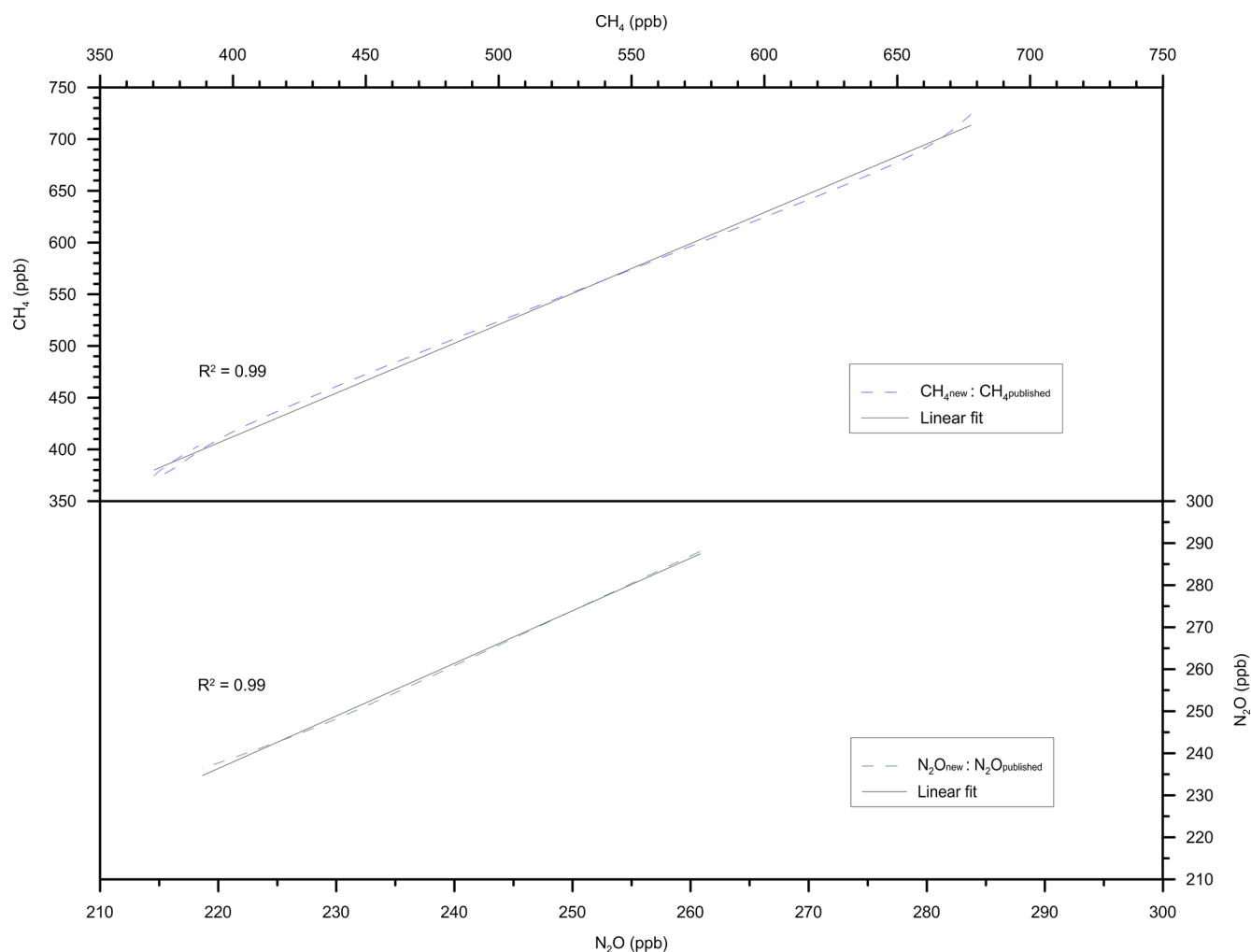


**Figure B1.** Offsets between new and published CH<sub>4</sub> and N<sub>2</sub>O EDC records. Dashed lines show the new measurements plotted against the published ones (data are from the spline approximations introduced in Appendix B). Solid lines are linear fits through these data.

**Data availability.** The new CH<sub>4</sub> and N<sub>2</sub>O data are available at the World Data Center for Paleoclimatology under the following link: <https://www.ncdc.noaa.gov/paleo/study/33673> (Schmidely et al., 2020).

**Author contributions.** The present study was designed by TFS, HF, and LoS. LoS and JH performed the methane and nitrous oxide measurements. JoS provided the isotopic data. LoS wrote the text with inputs from CNA, JoS, JH, LuS, JiS, FJ, JC, HF, and TFS.

**Competing interests.** The authors declare that they have no conflict of interest.

**Disclaimer.** Publisher's note: Copernicus Publications remains neutral with regard to jurisdictional claims in published maps and institutional affiliations.

**Acknowledgements.** The authors would like to thank Barbara Seth for the measurements of the isotopic composition of N<sub>2</sub>O, Gregory Teste for assistance in cutting ice samples, and Michael Bock and Jan Strähl for the construction of the new CH<sub>4</sub> and N<sub>2</sub>O measurement system. We thank the reviewers and the editor for detailed and constructive comments that improved this paper. We acknowledge financial support by the Swiss National Science Foundation (SNF project numbers 200020\_172745, 200020\_200492, 200020\_172506, 200020\_200511, and 200020\_159563). This work is a contribution to the European Project for Ice Coring in Antarctica (EPICA), a joint European Science Foundation/European Commission scientific programme, funded by the European Union and by national contributions from Belgium, Denmark, France, Germany, Italy, The Netherlands, Norway, Sweden, Switzerland, and the United Kingdom. The main logistic support was provided by IPEV and PNRA (at Dome C) and AWI (at Dronning Maud Land). This is EPICA publication no. 319. This project is TiPES (Tipping Points in the Earth System) contribution no. 125. This project has received funding from the European Union's Horizon 2020 research and innovation programme under grant 820970.

**Financial support.** This research has been supported by the Swiss National Science Foundation (SNF project numbers 200020\_172745, 200020\_172506, 200020\_159563, 200020\_200492 and 200020\_200511) and by the European Union's Horizon 2020 research and innovation programme (grant no. 820970).

**Review statement.** This paper was edited by Luke Skinner and reviewed by two anonymous referees.

## References

- Alley, R. B.: Wally was right: Predictive ability of the North Atlantic “conveyor belt” hypothesis for abrupt climate change, *Annu. Rev. Earth Pl. Sc.*, 35, 241–272, <https://doi.org/10.1146/annurev.earth.35.081006.131524>, 2007.
- Baumgartner, M., Schilt, A., Eicher, O., Schmitt, J., Schwander, J., Spahni, R., Fischer, H., and Stocker, T. F.: High-resolution inter-polar difference of atmospheric methane around the Last Glacial Maximum, *Biogeosciences*, 9, 3961–3977, <https://doi.org/10.5194/bg-9-3961-2012>, 2012.
- Baumgartner, M., Kindler, P., Eicher, O., Floch, G., Schilt, A., Schwander, J., Spahni, R., Capron, E., Chappellaz, J., Leuenberger, M., Fischer, H., and Stocker, T. F.: NGRIP CH<sub>4</sub> concentration from 120 to 10 kyr before present and its relation to a  $\delta^{15}\text{N}$  temperature reconstruction from the same ice core, *Clim. Past*, 10, 903–920, <https://doi.org/10.5194/cp-10-903-2014>, 2014.
- Bauska, T. K., Baggenstos, D., Brook, E. J., Mix, A. C., Marcott, S. A., Petrenko, V. V., Schaefer, H., Severinghaus, J. P., and Lee, J. E.: Carbon isotopes characterize rapid changes in atmospheric carbon dioxide during the last deglaciation, *P. Natl. Acad. Sci. USA*, 113, 3465–3470, <https://doi.org/10.1073/pnas.1513868113>, 2016.
- Bauska, T. K., Brook, E. J., Marcott, S. A., Baggenstos, D., Shackleton, S., Severinghaus, J. P., and Petrenko, V. V.: Controls on millennial-scale atmospheric CO<sub>2</sub> variability during the last glacial period, *Geophys. Res. Lett.*, 45, 7731–7740, <https://doi.org/10.1029/2018GL077881>, 2018.
- Bauska, T. K., Marcott, S. A., and Brook, E. J.: Abrupt changes in the global carbon cycle during the last glacial period, *Nat. Geosci.*, 14, 91–96, 2021.
- Bazin, L., Landais, A., Lemieux-Dudon, B., Toyé Mahamadou Kele, H., Veres, D., Parrenin, F., Martinerie, P., Ritz, C., Capron, E., Lipenkov, V., Loutre, M.-F., Raynaud, D., Vinther, B., Svensson, A., Rasmussen, S. O., Severi, M., Blunier, T., Leuenberger, M., Fischer, H., Masson-Delmotte, V., Chappellaz, J., and Wolff, E.: An optimized multi-proxy, multi-site Antarctic ice and gas orbital chronology (AICC2012): 120–800 ka, *Clim. Past*, 9, 1715–1731, <https://doi.org/10.5194/cp-9-1715-2013>, 2013.
- Beck, J., Bock, M., Schmitt, J., Seth, B., Blunier, T., and Fischer, H.: Bipolar carbon and hydrogen isotope constraints on the Holocene methane budget, *Biogeosciences*, 15, 7155–7175, <https://doi.org/10.5194/bg-15-7155-2018>, 2018.
- Berger, A. and Loutre, M.-F.: Insolation values for the climate of the last 10 million years, *Quaternary Sci. Rev.*, 10, 297–317, 1991.
- Bloom, A. A., Palmer, I. P., Fraser, A., Reay, D. S., and Frankenberg, C.: Large-scale controls of methanogenesis inferred from methane and gravity spaceborne data, *Science*, 327, 322–325, <https://doi.org/10.1126/science.1175176>, 2010.
- Bock, M., Schmitt, J., Möller, L., Spahni, R., Blunier, T., and Fischer, H.: Hydrogen isotopes preclude marine hydrate CH<sub>4</sub> emissions at the onset of Dansgaard–Oeschger events, *Science*, 328, 1686–1689, <https://doi.org/10.1126/science.1187651>, 2010.
- Bock, M., Schmitt, J., Beck, J., Seth, B., Chappellaz, J., and Fischer, H.: Glacial/interglacial wetland, biomass burning, and geologic methane emissions constrained by dual stable isotopic CH<sub>4</sub> ice core records, *P. Natl. Acad. Sci. USA*, 114, E5778–E5786, <https://doi.org/10.1073/pnas.1613883114>, 2017.

- Böhm, E., Lippold, J., Gutjahr, M., Frank, M., Blaser, P., Antz, B., Fohlmeister, J., Frank, N., Andersen, M. B., and Deininger, M.: Strong and deep Atlantic meridional overturning circulation during the last glacial cycle, *Nature*, 517, 73–76, <https://doi.org/10.1038/nature14059>, 2015.
- Broccoli, A. J., Dahl, K. A., and Stouffer, R. J.: Response of the ICTZ to Northern Hemisphere cooling, *Geophys. Res. Lett.*, 33, L01702, <https://doi.org/10.1029/2005GL024546>, 2006.
- Brook, E. J., Sowers, T., and Orchard, J.: Rapid variations in atmospheric methane concentration during the past 110,000 years, *Science*, 273, 1087–1091, 1996.
- Buizert, C. and Schmittner, A.: Southern Ocean control of glacial AMOC stability and Dansgaard-Oeschger interstadial duration, *Paleoceanography*, 30, 1595–1612, 2015.
- Cheng, H., Edwards, R. L., Wang, Y., Kong, X., Ming, Y., Kelly, M. J., Wang, X., Gallup, C. D., and Liu, W.: A penultimate glacial monsoon record from Hulu Cave and two-phase glacial terminations, *Geology*, 34, 217–220, <https://doi.org/10.1130/G22289.1>, 2006.
- Cheng, H., Edwards, R. L., Broecker, W. S., Denton, G. H., Kong, X., Wang, Y., Zhang, R., and Wang, X.: Ice age terminations, *Science*, 326, 248–252, <https://doi.org/10.1126/science.1177840>, 2009.
- Cheng, H., Edwards, R. L., Sinha, A., Spötl, C., Yi, L., Chen, S., Kelly, M., Kathayat, G., Wang, X., Li, X., Kong, X., Wang, Y., Ning, Y., and Zhang, H.: The Asian monsoon over the past 640,000 years and ice age terminations, *Nature*, 534, 640–646, <https://doi.org/10.1038/nature18591>, 2016.
- Deaney, E. L., Barker, S., and Van de Flierdt, T.: Timing and nature of AMOC recovery across Termination II and magnitude of deglacial CO<sub>2</sub> change, *Nat. Commun.*, 8, 14595, <https://doi.org/10.1038/ncomms14595>, 2017.
- Dlugokencky, E. J., Myers, R. C., Lang, P. M., Masarie, K. A., Crotwell, A. M., Thoning, K. W., Hall, B. D., Elkins, J. W., and Steele, L. P.: Conversion of NOAA atmospheric dry air CH<sub>4</sub> mole fractions to a gravimetrically prepared standard scale, *J. Geophys. Res.-Atmos.*, 110, D18306, <https://doi.org/10.1029/2005JD006035>, 2005.
- Dyonisius, M. N., Petrenko, V. V., Smith, A. M., Hua, Q., Yang, B., Schmitt, J., Beck, J., Seth, B., Bock, M., Hmiel, B., Vimont, I., Menking, J. A., Shackleton, S. A., Baggenstos, D., Bauska, T. K., Rhodes, R. H., Sperlich, P., Beaudette, R., Harth, C., Kalk, M., Brook, E. J., Fischer, H., Severinghaus, J. P., and Weiss, R. F.: Old carbon reservoirs were not important in the deglacial methane budget, *Science*, 367, 907–910, <https://doi.org/10.1126/science.aax0504>, 2020.
- Enting, I.: On the use of smoothing splines to filter CO<sub>2</sub> data, *J. Geophys. Res.-Atmos.*, 92, 10977–10984, <https://doi.org/10.1029/JD092iD09p10977>, 1987.
- Epifanio, J. A., Brook, E. J., Buizert, C., Edwards, J. S., Sowers, T. A., Kahle, E. C., Severinghaus, J. P., Steig, E. J., Winski, D. A., Osterberg, E. C., Fudge, T. J., Aydin, M., Hood, E., Kalk, M., Kreutz, K. J., Ferris, D. G., and Kennedy, J. A.: The SP19 chronology for the South Pole Ice Core – Part 2: gas chronology,  $\Delta$ age, and smoothing of atmospheric records, *Clim. Past*, 16, 2431–2444, <https://doi.org/10.5194/cp-16-2431-2020>, 2020.
- Fischer, H., Meissner, K. J., Mix, A. C., Abram, N. J., Auermann, J., Brovkin, V., Capron, E., Colombaroli, D., Danian, A.-L., Dyez, K. A., Felis, T., Finkelstein, S. A., Jaccard, S. L., McClymont, E. L., Rovere, A., Sutter, J., Wolff, E. W., Af-folter, S., Bakker, P., Ballesteros-Ctánovas, J. A., Barbante, C., Caley, T., Carlson, A. E., Churakova (Sidorova), O., Cortese, G., Cumming, B. F., Davis, B. A. S., de Vernal, A., Emile-Geay, J., Fritz, S. C., Gierz, P., Gottschalk, J., Holloway, M. D., Joos, F., Kucera, M., Loutre, M.-F., Lunt, D. J., Marcisz, K., Marlon, J. R., Martinez, P., Masson-Delmotte, V., Nehrbass-Ahles, C., Otto-Bliesner, B. L., Raible, C. C., Risebrobakken, B., Sánchez Goñi, M. F., Saleem Arrigo, J., Sarinthein, M., Sjolte, J., Stocker, T. F., Velasquez Álvarez, P. A., Tinner, W., Valdes, P. J., Vogel, H., Wanner, H., Yan, Q., Yu, Z., Ziegler, M., and Zhou, L.: Palaeoclimate constraints on the impact of 2 °C anthropogenic warming and beyond, *Nat. Geosci.*, 11, 474–485, <https://doi.org/10.1038/s41561-018-0146-0>, 2018.
- Fischer, H., Schmitt, J., Bock, M., Seth, B., Joos, F., Spahni, R., Lienert, S., Battaglia, G., Stocker, B. D., Schilt, A., and Brook, E. J.: N<sub>2</sub>O changes from the Last Glacial Maximum to the preindustrial – Part 1: Quantitative reconstruction of terrestrial and marine emissions using N<sub>2</sub>O stable isotopes in ice cores, *Biogeosciences*, 16, 3997–4021, <https://doi.org/10.5194/bg-16-3997-2019>, 2019.
- Flückiger, J., Dällenbach, A., Blunier, T., Stauffer, B., Stocker, T. F., Raynaud, D., and Barnola, J.-M.: Variations in atmospheric N<sub>2</sub>O concentration during abrupt climatic changes, *Science*, 285, 227–230, <https://doi.org/10.1126/science.285.5425.227>, 1999.
- Flückiger, J., Monnin, E., Stauffer, B., Schwander, J., Stocker, T. F., Chappellaz, J., Raynaud, D., and Barnola, J.-M.: High-resolution Holocene N<sub>2</sub>O ice core record and its relationship with CH<sub>4</sub> and CO<sub>2</sub>, *Global Biogeochem. Cy.*, 16, 10-1–10-8, <https://doi.org/10.1029/2001GB001417>, 2002.
- Flückiger, J., Blunier, T., Stauffer, B., Chappellaz, J., Spahni, R., Kawamura, K., Schwander, J., Stocker, T. F., and Dahl-Jensen, D.: N<sub>2</sub>O and CH<sub>4</sub> variations during the last glacial epoch: Insight into global processes, *Global Biogeochem. Cy.*, 18, GB1020, <https://doi.org/10.1029/2003GB002122>, 2004.
- Fourteau, K., Faïn, X., Martinerie, P., Landais, A., Ekaykin, A. A., Lipenkov, V. Ya., and Chappellaz, J.: Analytical constraints on layered gas trapping and smoothing of atmospheric variability in ice under low-accumulation conditions, *Clim. Past*, 13, 1815–1830, <https://doi.org/10.5194/cp-13-1815-2017>, 2017.
- Fourteau, K., Martinerie, P., Faïn, X., Ekaykin, A. A., Chappellaz, J., and Lipenkov, V.: Estimation of gas record alteration in very low-accumulation ice cores, *Clim. Past*, 16, 503–522, <https://doi.org/10.5194/cp-16-503-2020>, 2020.
- Grant, K. M., Rohling, E. J., Ramsey, B. C., Cheng, H., Edwards, R. L., Florindo, F., Heslop, D., Marra, F., Roberts, A. P., Tamisiea, M. E., and Williams, F.: Sea-level variability over five glacial cycles, *Nat. Commun.*, 5, 6076, <https://doi.org/10.1038/ncomms6076>, 2014.
- Guillevic, M., Bazin, L., Landais, A., Stowasser, C., Masson-Delmotte, V., Blunier, T., Eynaud, F., Falourd, S., Michel, E., Minster, B., Popp, T., Prié, F., and Vinther, B. M.: Evidence for a three-phase sequence during Heinrich Stadial 4 using a multiproxy approach based on Greenland ice core records, *Clim. Past*, 10, 2115–2133, <https://doi.org/10.5194/cp-10-2115-2014>, 2014.
- Hall, B. D., Dutton, G. S., and Elkins, J. W.: The NOAA nitrous oxide standard scale for atmospheric observations, *J. Geophys. Res.-Atmos.*, 112, D09305, <https://doi.org/10.1029/2006JD007954>, 2007.

- Hemming, S. R.: Heinrich events: Massive late Pleistocene detritus layers of the North Atlantic and their global climate imprint, *Rev. Geophys.*, 42, RG1005, <https://doi.org/10.1029/2003RG000128>, 2004.
- Hopcroft, P. O., Valdes, P. J., O'Connor, F. M., Kaplan, J. O., and Beerling, D. J.: Understanding the glacial methane cycle, *Nat. Commun.*, 8, 14383, <https://doi.org/10.1038/ncomms14383>, 2017.
- Joos, F., Battaglia, G., Fischer, H., Jeltsch-Thömmes, A., and Schmitt, J.: Marine N<sub>2</sub>O emissions during a Younger Dryas-like event: the role of meridional overturning, tropical thermocline ventilation, and biological productivity, *Environ. Res. Lett.*, 14, 075007, <https://doi.org/10.1088/1748-9326/ab2353>, 2019.
- Joos, F., Spahni, R., Stocker, B. D., Lienert, S., Müller, J., Fischer, H., Schmitt, J., Prentice, I. C., Otto-Bliesner, B., and Liu, Z.: N<sub>2</sub>O changes from the Last Glacial Maximum to the preindustrial – Part 2: terrestrial N<sub>2</sub>O emissions and carbon–nitrogen cycle interactions, *Biogeosciences*, 17, 3511–3543, <https://doi.org/10.5194/bg-17-3511-2020>, 2020.
- Jouzel, J., Masson-Delmotte, V., Cattani, O., Dreyfus, G., Falourd, S., Hoffmann, G., Minster, B., Nouet, J., Barnola, J.-M., Chappellaz, J., Fischer, H., Gallet, J. C., Johnsen, S., Leuenberger, M., Loulergue, L., Luethi, D., Oerter, H., Parrenin, F., Raisbeck, G., Raynaud, D., Schilt, A., Schwander, J., Selmo, E., Souchez, R., Spahni, R., Stauffer, B., Steffensen, J. P., Stenni, B., Stocker, T. F., Tison, J. L., Werner, M., and Wolff, E. W.: Orbital and millennial Antarctic climate variability over the past 800,000 years, *Science*, 317, 793–796, 2007.
- Landais, A., Dreyfus, G., Capron, E., Jouzel, J., Masson-Delmotte, V., Roche, D. M., Prié, F., Caillon, N., Chappellaz, J., Leuenberger, M., Laurantou, A., Parrenin, F., Raynaud, D., and Teste, G.: Two-phase change in CO<sub>2</sub>, Antarctic temperature and global climate during Termination II, *Nat. Geosci.*, 6, 1062–1065, <https://doi.org/10.1038/ngeo1985>, 2013.
- Levine, J. G., Wolff, E. W., Hopcroft, P. O., and Valdes, P. J.: Controls on the tropospheric oxidizing capacity during an idealized Dansgaard–Oeschger event, and their implications for the rapid rises in atmospheric methane during the last glacial period, *Geophys. Res. Lett.*, 39, L12805, <https://doi.org/10.1029/2012GL051866>, 2012.
- Loulergue, L., Schilt, A., Spahni, R., Masson-Delmotte, V., Blunier, T., Lemieux-Dudon, B., Barnola, J.-M., Raynaud, D., Stocker, T. F., and Chappellaz, J.: Orbital and millennial-scale features of atmospheric CH<sub>4</sub> over the past 800,000 years, *Nature*, 453, 383–386, <https://doi.org/10.1038/nature06950>, 2008.
- Marcott, S. A., Bauska, T. K., Buizert, C., Steig, E. J., Rosen, J. L., Cuffey, K. M., Fudge, T. J., Severinghaus, J. P., Ahn, J., Kalk, M. L., McConnell, J. R., Sowers, T., Taylor, K. C., White, J. W. C., and Brook, E. J.: Centennial-scale changes in the global carbon cycle during the last deglaciation, *Nature*, 514, 616–619, <https://doi.org/10.1038/nature13799>, 2014.
- Marino, G., Rohling, E. J., Rodríguez-Sanz, L., Grant, K. M., Heslop, D., Roberts, A. P., Stanford, J. D., and Yu, J.: Bipolar seesaw control on last interglacial sea level, *Nature*, 522, 197–201, <https://doi.org/10.1038/nature14499>, 2015.
- Melton, J. R., Wania, R., Hodson, E. L., Poulter, B., Ringeval, B., Spahni, R., Bohn, T., Avis, C. A., Beerling, D. J., Chen, G., Eliseev, A. V., Denisov, S. N., Hopcroft, P. O., Lettenmaier, D. P., Riley, W. J., Singarayer, J. S., Subin, Z. M., Tian, H., Zürcher, S., Brovkin, V., van Bodegom, P. M., Kleinen, T., Yu, Z. C., and Kaplan, J. O.: Present state of global wetland extent and wetland methane modelling: conclusions from a model inter-comparison project (WETCHIMP), *Biogeosciences*, 10, 753–788, <https://doi.org/10.5194/bg-10-753-2013>, 2013.
- Myhre, G., Shindell, D., Bréon, F.-M., Collins, W., Fuglestad, J., Huang, J., Koch, D., Lamarque, J.-F., Lee, D., Mendoza, B., Nakajima, T., Robock, A., Stephens, G., Takemura, T., and Zhang, H.: Anthropogenic and Natural Radiative Forcing, in: *Climate Change 2013: The Physical Science Basis. Contribution of Working Group I to the Fifth Assessment Report of the Intergovernmental Panel on Climate Change*, edited by: Stocker, T. F., Qin, D., Plattner, G.-K., Tignor, M., Allen, S. K., Boschung, J., Nauels, A., Xia, Y., Bex, V., and Midgley, P. M., Cambridge University Press, Cambridge, United Kingdom and New York, NY, USA, 2013.
- Nehrbass-Ahles, C., Shin, J., Schmitt, J., Bereiter, B., Joos, F., Schilt, A., Schmidely, L., Silva, L., Teste, G., Grilli, R., Chappellaz, J., Hodell, D., Fischer, H., and Stocker, T. F.: Abrupt CO<sub>2</sub> release to the atmosphere under glacial and early interglacial climate conditions, *Science*, 369, 1000–1005, <https://doi.org/10.1126/science.aay8178>, 2020.
- Nilsson-Kerr, K., Anand, P., Sexton, P. F., Leng, M. J., Misra, S., Clemens, S. C., and Hammond, S. J.: Role of Asian summer monsoon subsystems in the inter-hemispheric progression of deglaciation, *Nat. Geosci.*, 12, 290–295, <https://doi.org/10.1038/s41561-019-0319-5>, 2019.
- Oyabu, I., Kawamura, K., Kitamura, K., Dallmayr, R., Kitamura, A., Sawada, C., Severinghaus, J. P., Beaudette, R., Orsi, A., Sugawara, S., Ishidoya, S., Dahl-Jensen, D., Goto-Azuma, K., Aoki, S., and Nakazawa, T.: New technique for high-precision, simultaneous measurements of CH<sub>4</sub>, N<sub>2</sub>O and CO<sub>2</sub> concentrations; isotopic and elemental ratios of N<sub>2</sub>, O<sub>2</sub> and Ar; and total air content in ice cores by wet extraction, *Atmos. Meas. Tech.*, 13, 6703–6731, <https://doi.org/10.5194/amt-13-6703-2020>, 2020.
- Prather, M. J., Hsu, J., DeLuca, N. M., Jackman, C. H., Oman, L. D., Douglass, A. R., Fleming, E. L., Strahan, S. E., Steenrod, S. D., Søvde, O. A., Isaksen, I. S. A., Froidevaux, P., and Funke, B.: Measuring and modeling the lifetime of nitrous oxide including its variability, *J. Geophys. Res.-Atmos.*, 120, 5693–5705, <https://doi.org/10.1002/2015JD023267>, 2015.
- Rhodes, R. H., Brook, E. J., Chiang, J. C. H., Blunier, T., Maselli, O. J., McConnell, J. R., Romanini, D., and Severinghaus, J. P.: Enhanced tropical methane production in response to ice-berg discharge in the North Atlantic, *Science*, 348, 1016–1019, <https://doi.org/10.1126/science.1262005>, 2015.
- Rhodes, R. H., Fain, X., Brook, E. J., McConnell, J. R., Maselli, O. J., Sigl, M., Edwards, J., Buizert, C., Blunier, T., Chappellaz, J., and Freitag, J.: Local artifacts in ice core methane records caused by layered bubble trapping and in situ production: a multi-site investigation, *Clim. Past*, 12, 1061–1077, <https://doi.org/10.5194/cp-12-1061-2016>, 2016.
- Rosen, J. L., Brook, E. J., Severinghaus, J. P., Blunier, T., Mitchell, L. E., Lee, J. E., Edwards, J. S., and Gkinis, V.: An ice core record of near-synchronous global climate changes at the Bølling transition, *Nat. Geosci.*, 7, 459–463, <https://doi.org/10.1038/ngeo2147>, 2014.
- Schilt, A., Baumgartner, M., Blunier, T., Schwander, J., Spahni, R., Fischer, H., and Stocker, T. F.: Glacial–interglacial and

- millennial-scale variations in the atmospheric nitrous oxide concentration during the last 800,000 years, *Quaternary Sci. Rev.*, 29, 182–192, <https://doi.org/10.1016/j.quascirev.2009.03.011>, 2010a.
- Schilt, A., Baumgartner, M., Schwander, J., Buiron, D., Capron, E., Chappellaz, J., Loulergue, L., Schüpbach, S., Spahni, R., Fischer, H., and Stocker, T. F.: Atmospheric nitrous oxide during the last 140,000 years, *Earth Planet. Sc. Lett.*, 300, 33–43, <https://doi.org/10.1016/j.epsl.2010.09.027>, 2010b.
- Schilt, A., Baumgartner, M., Eicher, O., Chappellaz, J., Schwander, J., Fischer, H., and Stocker, T. F.: The response of atmospheric nitrous oxide to climate variations during the last glacial period, *Geophys. Res. Lett.*, 40, 1888–1893, <https://doi.org/10.1002/grl.50380>, 2013.
- Schilt, A., Brook, E. J., Bauska, T. K., Baggenstos, D., Fischer, H., Joos, F., Petrenko, V. V., Schaefer, H., Schmitt, J., Severinghaus, J. P., Spahni, R., and Stocker, T. F.: Isotopic constraints on marine and terrestrial N<sub>2</sub>O emissions during the last deglaciation, *Nature*, 516, 234–237, <https://doi.org/10.1038/nature13971>, 2014.
- Schmidely, L., Nehrbass-Ahles, C., Schmitt, J., Han, J., Silva, L., Shin, J., Joos, F., Chappellaz, J., Fischer, H., and Stocker, T. F.: CH<sub>4</sub> and N<sub>2</sub>O fluctuations during the penultimate deglaciation, *Climate of the Past Discussions*, NOAA [data set], available at: <https://www.ncdc.noaa.gov/paleo/study/33673> (last access: 29 July 2021), 2020.
- Schmitt, J., Seth, B., Bock, M., and Fischer, H.: Online technique for isotope and mixing ratios of CH<sub>4</sub>, N<sub>2</sub>O, Xe and mixing ratios of organic trace gases on a single ice core sample, *Atmos. Meas. Tech.*, 7, 2645–2665, <https://doi.org/10.5194/amt-7-2645-2014>, 2014.
- Schmittner, A. and Galbraith, E. D.: Glacial greenhouse-gas fluctuations controlled by ocean circulation changes, *Nature*, 456, 373–376, <https://doi.org/10.1038/nature07531>, 2008.
- Skinner, L. C. and Shackleton, N. J.: Deconstructing Terminations I and II: revisiting the glacioeustatic paradigm based on deep-water temperature estimates, *Quaternary Sci. Rev.*, 25, 3312–3321, <https://doi.org/10.1016/j.quascirev.2006.07.005>, 2006.
- Sowers, T.: N<sub>2</sub>O record spanning the penultimate deglaciation from the Vostok ice core, *J. Geophys. Res.-Atmos.*, 106, 31903–31914, <https://doi.org/10.1126/science.1121235>, 2001.
- Spahni, R., Chappellaz, J., Stocker, T. F., Loulergue, L., Hausamann, G., Kawamura, K., Flückiger, J., Schwander, J., Raynaud, D., and Masson-Delmotte, V.: Atmospheric methane and nitrous oxide of the late Pleistocene from Antarctic ice cores, *Science*, 310, 1317–1321, <https://doi.org/10.1126/science.1120132>, 2005.
- Van Groenigen, K. J., Osenberg, C. W., and Hungate, B. A.: Increased soil emissions of potent greenhouse gases under increased atmospheric CO<sub>2</sub>, *Nature*, 475, 214–216, <https://doi.org/10.1038/nature10176>, 2011.
- Veres, D., Bazin, L., Landais, A., Toyé Mahamadou Kele, H., Lemieux-Dudon, B., Parrenin, F., Martinerie, P., Blayo, E., Blunier, T., Capron, E., Chappellaz, J., Rasmussen, S. O., Severi, M., Svensson, A., Vinther, B., and Wolff, E. W.: The Antarctic ice core chronology (AICC2012): an optimized multi-parameter and multi-site dating approach for the last 120 thousand years, *Clim. Past*, 9, 1733–1748, <https://doi.org/10.5194/cp-9-1733-2013>, 2013.